25 W single-frequency, low noise fiber MOPA at 1120 nm

Benoît Gouhier, Germain Guiraud, Sergio Rota-Rodrigo, Jian Zhao, Nicholas Traynor, Giorgio Santarelli

25 W single-frequency, low noise fiber MOPA at 1120 nm

BENOÎT GOUHIER,[1*] GERMAIN GUIRAUD,[1,2] SERGIO ROTA-RODRIGO,[1] JIAN ZHAO,[1] NICHOLAS TRAYNOR[2] AND GIORGIO SANTARELLI[1]

[1] Laboratoire Photonique, Numérique et Nanosciences, Institut d'Optique Graduate School, CNRS, Université de Bordeaux, Talence, France
[2] Azur Light Systems, Avenue de la Canteranne, Pessac, France
*Corresponding author: benoit.gouhier@institutoptique.fr

This letter reports on the development of a 25 W single-frequency, all-fiber master-oscillator power amplifier operating at 1120 nm. By heating the gain fiber at 75 °C, an output power of 25.3 W is achieved with an optical-to-optical efficiency of 53.5 %. The output shows no sign of stimulated Brillouin scattering and the signal to amplified spontaneous emission ratio is close to 40 dB. A M^2 value of 1.15 and a polarization extinction ratio of 17 dB are measured. The relative intensity noise of the output is also characterized, reaching -155 dBc/Hz at 10MHz at the maximum output power. The study of the noise dynamics highlights for the first time to the best of our knowledge an unpredicted behavior due to the strong backward amplified spontaneous emission.

Single-frequency (SF) Ytterbium (Yb) fiber lasers are gaining popularity for cutting-edge research such as gravitational wave detectors [1], coherent beam combining [1,2] or atom trapping and cooling [3]. Indeed, such applications demand a high-power, low noise signal with near diffraction-limited modal properties and excellent pointing stability, which fiber lasers can deliver easily due to their monolithic nature and good thermal management. Fiber's ability to handle high powers fits particularly well the master oscillator power amplifier (MOPA) architecture, where the signal from a low-noise seed is boosted through one or several stages of amplification. This approach has led to the development of several SF, low-noise, hundred-watt class lasers [4–6].

However, despite the very wide emission spectrum of Yb (970–1200 nm), powerful lasers emitting outside of the conventional band (1020–1090 nm) remain sparse. Of particular interest is the L-band of Yb gain spectrum (beyond 1120 nm), both for tandem pumping of Holmium-doped lasers [7] or Raman lasers at 1178 nm [8]. In addition, the yellow light obtained by frequency-doubling has many applications in atom cooling, cytometry, holography and ophthalmology [9–11].

Yb-doped fiber lasers have already been demonstrated at these exotic wavelengths. With a long cavity of large mode area (LMA) fiber between two fiber Bragg gratings (FBG), several hundreds of Watts of output power have been obtained beyond 1100 nm [12–14]. Because of the low emission cross-section, it is necessary to deal with the strong gain competition between signal and amplified spontaneous emission (ASE) around 1030 nm. To this end, photonic bandgap (PBG) fiber has been implemented at 1178nm [15], but its usage remains confined to specific cases, and it has yet to be demonstrated in a monolithic system. Raman lasers have also proven a successful alternative to generate wavelengths beyond 1100 nm [16,17].

These approaches are however unfit for high-power SF operation. For fiber oscillators, the necessarily short cavity strongly limits the gain. The only SF fiber laser demonstrated so far at this wavelength can indeed only deliver 60 mW from a 31 mm-long cavity [18]. When operating in SF regime, Raman lasers suffer from stimulated Brillouin scattering (SBS) which thrives in these conditions (long gain medium, SF operation). Typical solutions
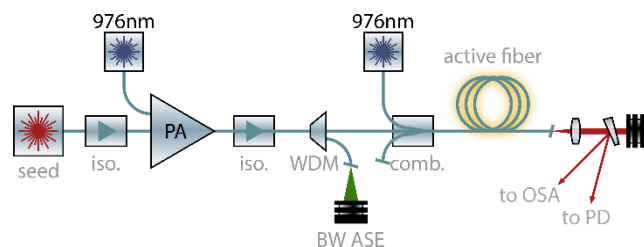

Fig. 1: Schematic of the all-fiber MOPA. Iso.: isolator; PA: Pre-amplifier; WDM: Wavelength-division multiplexer; comb.: Pump combiner; OSA: Optical Spectrum Analyzer; PD: Photodiode; BW ASE: Backward-propagating Amplified Spontaneous Emission
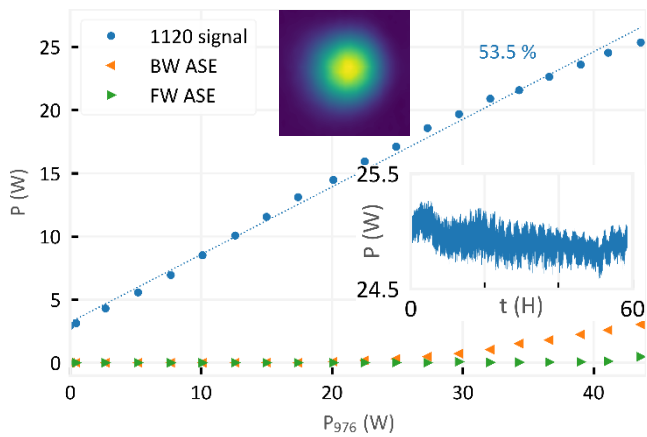
Fig. 2: Output signal and ASE power vs. launched pump power. Insets show mode profile and power stability over 60 hours

imply acoustic tailoring of the fiber core to mitigate acousto-optical interaction [19], as well as applying temperature or strain gradients to modify Brillouin gain over different fiber sections [8,20,21]. The latter method is also popular in SF MOPA lasers [6]. Although simple in principle, these solutions remain tedious to implement and impairs reliability and reproducibility of the system. As we aim to realize an industrial-grade laser in the long term, we chose to avoid these solutions. To date, the highest power reported for a SF, all-fiber laser at 1120 nm is 2 W [22]. Semiconductor diodes also fail to overcome the 10 W barrier [9,23].

In this paper, we report on an all-fiber, low-noise, SF, 25 W MOPA laser operating at 1120 nm. Parasitic lasing around 1040 nm is avoided by heating the fiber at 75 °C, and the output signal shows no sign of SBS, which is the main limiting factor for this type of laser [24]. The output beam shows outstanding modal features (M<1.15) and an excellent Polarization Extinction Ratio (PER) of 17dB.

The schematic of the fiber MOPA is shown in Fig. 1. The seed laser is a SF Distributed Feed-Back (DFB) laser diode (QDLaser QLD1161-2030) emitting up to 70 mW at 1120 nm. The fast linewidth was estimated to be below 300 kHz by heterodyne beating with an identical laser diode. The seed laser was spliced to an isolator which i) protects it against back reflections, and ii) strongly attenuates backward (BW) ASE from the MOPA. The pre-amplifier is based on conventional 10 μm Yb-doped polarization-maintaining (PM) fiber (Nufern PLMA-YDF-10/125-VIII), which has a specified clad absorption of 4.8 dB/m at 976 nm. The power
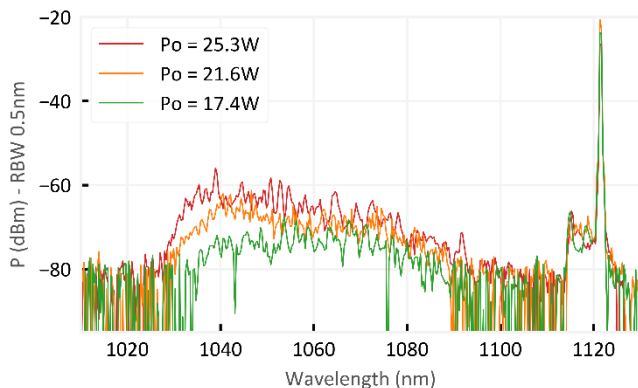
at the output of the pre-amplifier can reach up to 5 W. Again, an isolator was spliced at the output of the pre-amplifier to avoid back-reflections. Also, to discard the strong BW ASE from the main stage, a wavelength-division multiplexer (WDM) was inserted just after the isolator. The main stage consists of 5 m of PM LMA fiber with a mode field diameter (MFD) of 15 μm and a clad diameter of approximately 130 μm. With less than 0.5% of residual pump detected at the output (measured after a dichroic mirror), the effective clad absorption is 4.6 dB/m. The fiber must be kept short to avoid SBS, but long enough to ensure reabsorption of co-propagating ASE at the end of the fiber. The active fiber was mounted on a heating plate and its temperature was maintained at 75 °C. Heating is known to enhance the absorption coefficient of short wavelengths [25,26]. In this case, it enables to favor gain at 1120 nm rather than around 1030 nm, leading to a dramatic reduction of the ASE. Heating is usually best avoided as it affects the lifetime of fibers, since the coating polymer of conventional double-clad fibers does not deal well with high temperatures. Here, we chose not to heat over 75 °C to preserve the fiber long term integrity. By using active fibers with air-clad, pump guiding would not be affected by a degradation of the coating polymer, and we could in principle further decrease ASE by heating at higher temperatures. A fraction of the output signal was extracted so that the output spectrum could be observed with an optical spectrum analyzer (OSA). The power of the BW ASE was also monitored at the reflective output of the WDM.

The output power at 1120 nm against the launched pump power is shown in Fig. 2, together with the forward (FW) and BW ASE. The power of the FW ASE was computed from the output spectrum. The maximum output power of 25.3 W is reached for a launched pump power of 43.6 W, with an overall efficiency of 53.5 %. The curve starts to saturate at around 21 W () because of the growing BW ASE, which reaches 3.5 W at maximum pump. However, the FW ASE remains below 500 mW. The performance of our main amplifier is on-par with similar works [13,14]. A stronger seed power would however be helpful to further improve efficiency.

The stability of the output power was monitored for close to 60 hours (Fig. 2 inset). Power fluctuations reached 2.7% peak-to-peak, and were found to closely follow room temperature. The beam profile was observed and is also shown in Fig. 2. The M^2 value was measured to be less than 1.15. The polarization extinction ratio was more than 17 dB at the maximum power, with less than 0.5 dB of variation over an hour.
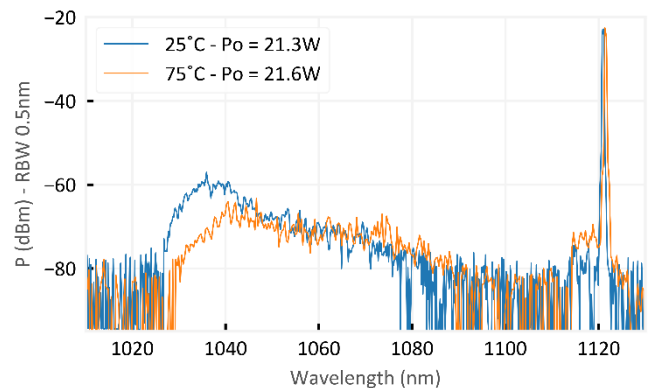

Fig. 3: Output signal spectrum for different output powers.

Fig. 4: Effect of heating on output spectrum (P_{pump}=35 W).

The spectra for different pump powers are plotted in Fig. 3. The extinction ratio is close to 40 dB at maximum power. With increasing pump power, the peak of the ASE shifts towards shorter wavelengths. Indeed, as the end of the fiber gradually sees more pump, absorption of short wavelengths decreases. At the maximum output power, the ASE bandwidth spans over 60 nm. However, it sits more than 30 nm away from the signal wavelength, meaning that can be easily filtered out with an adapted dichroic filter. Because the bandwidth of the WDM is about 10 nm, some ASE from the preamplifier was fed into the final stage and amplified, causing the pedestal around 1120 nm (see Fig. 3). Filtering out this noise is more difficult. A solution would be to use a more selective WDM at the output of the pre-amplifier. Regardless, its level remains low, at around 50 dB below the signal.

Spectral broadening arising from self-phase modulation and four-wave-mixing [27] is a common concern for high-power doped-fiber laser and amplifiers, where the multiple longitudinal modes interact to generate new optical frequencies. In SF regime however, these effects are not as troublesome as only one longitudinal mode is present. In addition, multiple previous works have shown that the amplification process does not add any excess phase noise to the seed laser [28–30]. From these, we can safely conclude that the spectral properties of the previously characterized seed laser are maintained throughout the amplifier.

The effect of heating on the output spectrum is shown in Fig. 4. The blue curve corresponds to the fiber being heated at 25 °C, and the orange one at 75 °C. In the same conditions (4 W seed, 35 W pump) the output power remains constant (resp. 21.3 W and 21.6 W), but the shape and integrated power of the ASE is dramatically affected. Indeed, the gain around 1030 nm is reduced by more than 15 dB when the fiber is heated at 75 °C. The wavelengths in the 1050–1100 nm window see little change. Although heating does not improve the overall efficiency, the strong ASE absorption prevents early parasitic lasing, allowing for more pump power to be launched.

To check for the presence of SBS, we rely on observation of the relative intensity noise (RIN) of the output. SBS signature is a white noise at high frequency, typically above 1 MHz [31]. The RIN of the output signal was then measured for different powers. The results are shown in Fig. 5. Above 1 MHz, the noise level does not increase with power, ruling out the presence of SBS. The RIN remains below -120 dBc/Hz above 1 kHz, and goes down to -155 dBc/Hz at 10 MHz.
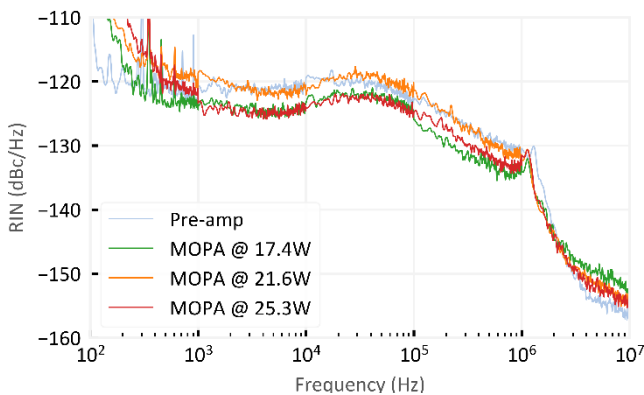
In addition to SBS, other noise sources have an impact on the output RIN. To fully characterize the intensity noise of the laser, we must study the RIN more closely. Noise dynamics of MOPA fiber lasers are well understood. Accurate models have been developed for Erbium (Er) amplifiers, and later successfully adapted to Yb amplifiers under certain conditions (large gain, low spontaneous emission) [32–34]. These models describe the contribution of pump and seed noise to the RIN of the output signal of a fiber MOPA, and derive the equations of the transfer functions (TF) of pump and seed power fluctuations to the MOPA output. Basically, the former responds as a low pass filter while the latter behaves as a damped high pass filter. The transition between these two processes happens at a corner frequency which mainly depends on output power, fiber core radius and absorption/emission cross-sections. From these models, we can discriminate the different contributors to the RIN of the output signal. To this end, RIN measurements of the pre-amplifier (which seeds the main amplification stage) and of the 50 W pump diode were performed between 100 Hz and 10 MHz. Based on the standard MOPA RIN models mentioned previously, the zero and corner frequencies of the seed and pump noise transfer functions can be calculated. This calculation strongly depends on the emission cross-section at 1120 nm, which is not well characterized in the literature. From the data in [35], this value was then estimated as eight times lower than the 1064 nm coefficient. From there, the corner frequency at 12, 18 and 25 W output power were respectively found to be 1.9, 2.9 and 4.1 kHz (see [34] for methods). For comparison, the actual transfer function of the pump through the main stage was also measured by direct modulation of an auxiliary pump. The results are shown in Fig. 6.

Unexpectedly, the measurements do not match the theoretical model. Instead of behaving as a simple low pass filter, the pump TF seems to exhibit two poles at different frequencies. This behavior was never observed before in rare-earth doped fiber MOPAs, being whether Er [33], Yb [33,34], Neodymium [36] or Thulium [in preparation]. After fitting to a dual-pole low pass filter, we find that the first frequency matches the theoretical value, while the second one sits roughly a decade higher. In addition, the gain associated with this second corner frequency quickly increases with output power (which is illustrated by the raise of the plateau around 10 kHz in Fig. 6). This unexpected behavior indicates an additional phenomenon modifies the pump TF. A potential explanation is the presence of significant ASE which is neglected in theoretical models. These were indeed designed to emulate operation in the

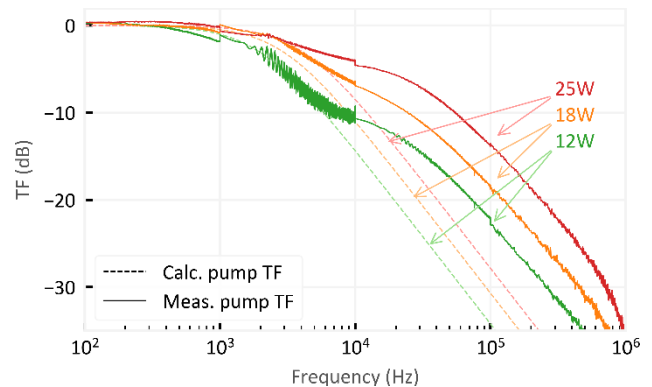Fig. 5: Measured RINs of the preamp and MOPA for different output powers (detected optical power 10 mW).

Fig. 6: Calculated and measured transfer functions for pump modulation.

conventional band of Er (1530-1565 nm [32]) and Yb (1020-1080 nm [33]) where ASE is not an issue. We assume that the strong BW ASE affects pump depletion and signal gain at the beginning of the fiber, causing intertwined energy transfers which impact the pump TF in a non-trivial way. In addition, the FW ASE that gets reabsorbed at the end of the gain fiber acts as a 1030 nm-pump in the fiber core, again affecting the behavior of the amplifier. After additional measurements at lower seed powers (not reported), we indeed found that the gain of the second transfer function was strongly correlated to the ASE level. However, a deeper, more systematic study is needed to fully characterize this complex behavior, and falls beyond the scope of this paper. For now, we can conclude that this additional process will make noise-reducing feedback mechanisms difficult to implement, not only because of the higher free-running noise induced by the pump and ASE, but also because of the complex response of the system to pump fluctuations.

In summary, we have developed a 25 W all-fiber, SBS-free, SF MOPA operating at 1120 nm. At 25 W, the output signal exhibits a 40 dB ASE extinction ratio, low RIN, good long-term power and polarization stability as well as excellent modal properties. No excess noise was detected above 1 MHz, ruling out the presence of SBS. RIN at lower frequency is dominated by seed- (here preamp) and pump-induced noise. However, because of the strong level of ASE, pump TF was found to exhibit a behavior not predicted by conventional models developed for Er/Yb MOPAs. This observation forecasts a challenging noise reduction for MOPAs operating outside of the conventional band. Further power scaling would be difficult, given the fast rise of ASE. To achieve this, either stronger heating (with the risk of damaging the fiber) or an additional stage would need to be implemented. In-band core-pumping could also be implemented as in [37], although the use of a noisy fiber laser as pump may hamper the output RIN. This new SF MOPA is an ideal candidate for the generation of frequency-doubled high-power low noise light at 560 nm.

References

1. L.-W. Wei, F. Cleva, and C. N. Man, Opt. Lett. **41**, 5817–5820 (2016).
2. Z. Liu, P. Zhou, X. Xu, X. Wang, and Y. Ma, Sci. China Technol. Sci. **56**, 1597–1606 (2013).
3. M. N. Zervas and C. A. Codemard, IEEE J. Sel. Top. Quantum Electron. **20**, 219–241 (2014).
4. S. Fu, W. Shi, Y. Feng, L. Zhang, Z. Yang, S. Xu, X. Zhu, R. A. Norwood, and N. Peyghambarian, JOSA B **34**, A49–A62 (2017).
5. G. Guiraud, N. Traynor, and G. Santarelli, Opt. Lett. **41**, 4040–4043 (2016).
6. L. Huang, H. Wu, R. Li, L. Li, P. Ma, X. Wang, J. Leng, and P. Zhou, Opt. Lett. **42**, 1–4 (2017).
7. A. S. Kurkov, V. V. Dvoyrin, and A. V. Marakulin, Opt. Lett. **35**, 490–492 (2010).
8. L. Zhang, H. Jiang, S. Cui, J. Hu, and Y. Feng, Laser Photonics Rev. **8**, 889–895 (2014).
9. A. K. Hansen, M. Christensen, D. Noordegraaf, P. Heist, E. Papastathopoulos, V. Loyo-Maldonado, O. B. Jensen, and P. M. W. Skovgaard, Appl. Opt. **55**, 9270–9274 (2016).
10. V. Kapoor, V. Karpov, C. Linton, F. V. Subach, V. V. Verkhusha, and W. G. Telford, Cytometry A **73A**, 570–577 (2008).
11. S. Uetake, A. Yamaguchi, S. Kato, and Y. Takahashi, Appl. Phys. B **92**, 33–35 (2008).
12. H. Zhang, H. Xiao, P. Zhou, X. Wang, and X. Xu, IEEE Photonics Technol. Lett. **25**, 2093–2096 (2013).
13. L. Huang, H. Zhang, X. Wang, R. Su, and P. Zhou, Laser Phys. **26**, 075105 (2016).
14. H. Xiao, H. Zhang, J. Xu, J. Leng, and P. Zhou, JOSA B **34**, A63–A69 (2017).
15. A. Shirakawa, H. Maruyama, K. Ueda, C. B. Olausson, J. K. Lyngsø, and J. Broeng, Opt. Express **17**, 447–454 (2009).
16. H. Zhang, R. Tao, P. Zhou, X. Wang, and X. Xu, IEEE Photonics Technol. Lett. **27**, 628–630 (2015).
17. C. A. Codemard, J. Ji, J. K. Sahu, and J. Nilsson, in *Proc. of SPIE* (2010), Vol. 7580, p. 75801N.
18. C. Yang, Q. Zhao, Z. Feng, M. Peng, Z. Yang, and S. Xu, Opt. Express **24**, 29794–29799 (2016).
19. I. Dajani, C. Vergien, C. Robin, and B. Ward, Opt. Express **21**, 12038–12052 (2013).
20. V. R. Supradeepa, Y. Feng, and J. W. Nicholson, J. Opt. **19**, 023001 (2017).
21. L. Taylor, Y. Feng, and D. B. Calia, Opt. Express **17**, 14687–14693 (2009).
22. A. Friedenauer, F. Markert, H. Schmitz, L. Petersen, S. Kahra, M. Herrmann, T. Udem, T. W. Hänsch, and T. Schätz, Appl. Phys. B **84**, 371–373 (2006).
23. K. Paschke, C. Fiebig, G. Blume, F. Bugge, J. Fricke, and G. Erbert, in *Proc. SPIE* (2013), Vol. 8640, p. 86401J.
24. A. Yeniay, J. M. Delavaux, and J. Toulouse, J. Light. Technol. **20**, 1425–1432 (2002).
25. D. A. Grukh, A. S. Kurkov, V. M. Paramonov, and E. M. Dianov, Quantum Electron. **34**, 579–582 (2004).
26. M. Jacquemet, A. Mugnier, G. L. Corre, E. Goyat, and D. Pureur, IEEE J. Sel. Top. Quantum Electron. **15**, 120–128 (2009).
27. S. I. Kablukov, E. A. Zlobina, E. V. Podivilov, and S. A. Babin, Opt. Lett. **37**, 2508–2510 (2012).
28. I. Ricciardi, S. Mosca, P. Maddaloni, L. Santamaria, M. D. Rosa, and P. D. Natale, Opt. Express **21**, 14618–14626 (2013).
29. M. Tröbs, S. Barke, T. Theeg, D. Kracht, G. Heinzel, and K. Danzmann, Opt. Lett. **35**, 435–437 (2010).
30. N. Chiodo, K. Djerroud, O. Acef, A. Clairon, and P. Wolf, Appl. Opt. **52**, 7342–7351 (2013).
31. M. Hildebrandt, S. Buesche, P. Wessels, M. Frede, and D. Kracht, Opt. Express **16**, 15970 (2008).
32. S. Novak and A. Moesle, J. Light. Technol. **20**, 975 (2002).
33. H. Tünnermann, J. Neumann, D. Kracht, and P. Weßels, Opt. Express **20**, 13539 (2012).
34. J. Zhao, G. Guiraud, F. Floissat, B. Gouhier, S. Rota-Rodrigo, N. Traynor, and G. Santarelli, Opt. Express **25**, 357–366 (2017).
35. A. S. Kurkov, Laser Phys. Lett. **4**, 93–102 (2007).
36. S. Rota-Rodrigo, B. Gouhier, M. Laroche, J. Zhao, B. Canuel, A. Bertoldi, N. Traynor, B. Cadier, T. Robin, and G. Santarelli, Opt. Lett. **42**, (2017).
37. T. Theeg, C. Ottenhues, H. Sayinc, J. Neumann, and D. Kracht, Opt. Lett. **41**, 9 (2016).